ISSN: 2639-7455

Research Article

Earth & Environmental Science Research & Reviews

Unraveling the Geothermal Potential of Corbetti Caldera Using Integrated Geophysical Methods, Central Main Ethiopian Rift

Bisrat Kebede[1, 2]*, Abera Alemu[1], Hailemichael Kebede[3], Enatfenta Melaku[2], Dejene Feyissa[4], Guta Legesse[2]

[1]*School of Earth Science, Addis Ababa University, P.O. Box 1176, Addis Ababa, Ethiopia*

[2]*Mineral Industry Development Institute, P.O. Box 486, Addis Ababa, Ethiopia*

[3]*Computational Data Science Program, Addis Ababa University, P.O. Box 1176, Addis Ababa, Ethiopia*

[4]*Geological Institute of Ethiopia, P.O. Box 486, Addis Ababa, Ethiopia*

***Corresponding Author**
Bisrat Kebede, School of Earth Science, Addis Ababa University, P.O. Box 1176, Addis Ababa, Ethiopia

Submitted: 13 Dec 2022; **Accepted:** 20 Dec 2022; **Published:** 05 Jan 2023

Citation: Kebede B*, Alemua A, Kebedec H, Melakub E, Feyissad D, Legesseb G. (2023). Unraveling the Geothermal Potential of Corbetti Caldera Using Integrated Geophysical Methods, Central Main Ethiopian Rift.). *Eart & Envi Scie Res & Rev*. 6(1): 333-351.

Abstract

In this paper integrated geophysical techniques, involving electrical resistivity, gravity and magnetic surveys have been carried out over the Corbetti Caldera in the central Main Ethiopian Rift (CMER) to verify the geothermal potential of the caldera. Corbetti geothermal prospect is located at about 250 km south of Addis Ababa and 20km from Awassa city and the area is bounded by Lake Awassa to the south and Lake Shalla to the north with geographic location between latitude 7.170N-7.250N and longitudes 38.300E-38.470E. The Corbetti Caldera is characterized by Quaternary volcano-tectonic activity which is mainly silicic volcanism and a resurgent caldera structural system. Quaternary volcanism is associated with a wide spread of steaming ground and fumarolic activity which could confirm the existence of a heat source at depth. Fifty six (56) VES points, 200 gravity and about 200 magnetic data have been used and analyzed. The results are presented as magnetic, gravity and electrical counter maps for qualitative interpretation. Constrained gravity and magnetic 2D model and results obtained from the geoelectric section were made for quantitative interpretation. The complete Bouguer gravity anomaly in conjugation with the total magnetic field anomaly map of the area indicates the existence of intrusion beneath the caldera, i.e. the highest Bouguer gravity anomaly resulting from the higher density of the intrusion. Correspondingly the shallower heat source caused by this intrusion is characterized by the lowest magnetic anomaly response. Results from vertical electrical soundings along profile-2 indicate the presence of a middle thicker conductive zone which is associated with the increase in temperature and alteration of rocks. Apparent resistivity map for AB/2=1810m and AB/2=2700m shows low resistivity anomaly follows the eastern and northern caldera rim, stretching north of the caldera towards Lake Shalla.

Keywords: Geothermal, Volcano, Caldera, intrusion, Rift, Magmatic Segment

Introduction

The Main Ethiopian Rift (MER) which is part of the East African Rift system (EARS) where rifting began as early as late Oligocene-early Miocene times and composed of three main segments; northern, central, and southern MER in which the divisions of these segments are marked by E-W trending transverse structures, the Goba-Bonga lineament separating the central MER from the southern MER and the Yerer-Tullu Wellel volcano-tectonic lineament (YTVTL) is a boundary between the northern and the central MER [1-6]. The Main Ethiopian Rift (MER), being one segment of the East African continental rift system is characterized by recent volcano-tectonic features (central volcanoes, calderas, craters, cones, faults, grabens, etc), intense seismic activity and zones of mineralization with possible shallow intrusions. Several Quaternary central volcanoes namely Corbetti, Aluto, Gedemsa, Dofan...etc (Fig 1) are located along the axial portion of the MER [7, 8]. These central volcanoes offered opportunities for potential geothermal resource investigations(H. Kebede et al., 2022) and the Corbetti volcano, a central volcanic complex in the MER, is among those promoted for detailed geothermal resources investigation. The central sector of MER, where the Hawassa lake basin belongs to is a symmetric rift basin where both sides of the rift margins are fully defined except in the region between Guraghe and Sodo of the western escarpment and the Shashemene area of the eastern margin and the closed basin of the nested Hawassa-Corbetti caldera complex is a giant elliptical depression 30-40kms wide [9-13].

Ethiopia is one of the developing countries in sub-Saharan Africa with a high level of household energy consumption primar-

ily satisfied through excessive burning of biomass [14-16]. Although Ethiopia has estimated exploitable geothermal potential of around 5000 MW on the rift environment, currently this potential is largely untapped and only a pilot project of 7.5 MW has been installed at Aluto Langano and 10 MW and pilot projects is under construction at Tendaho Dubti [17-19]. Additionally, Corbetti, Abaya, Dofan Fantale and Tulu Moye areas are being surface explored for future geothermal prospects [20, 21].

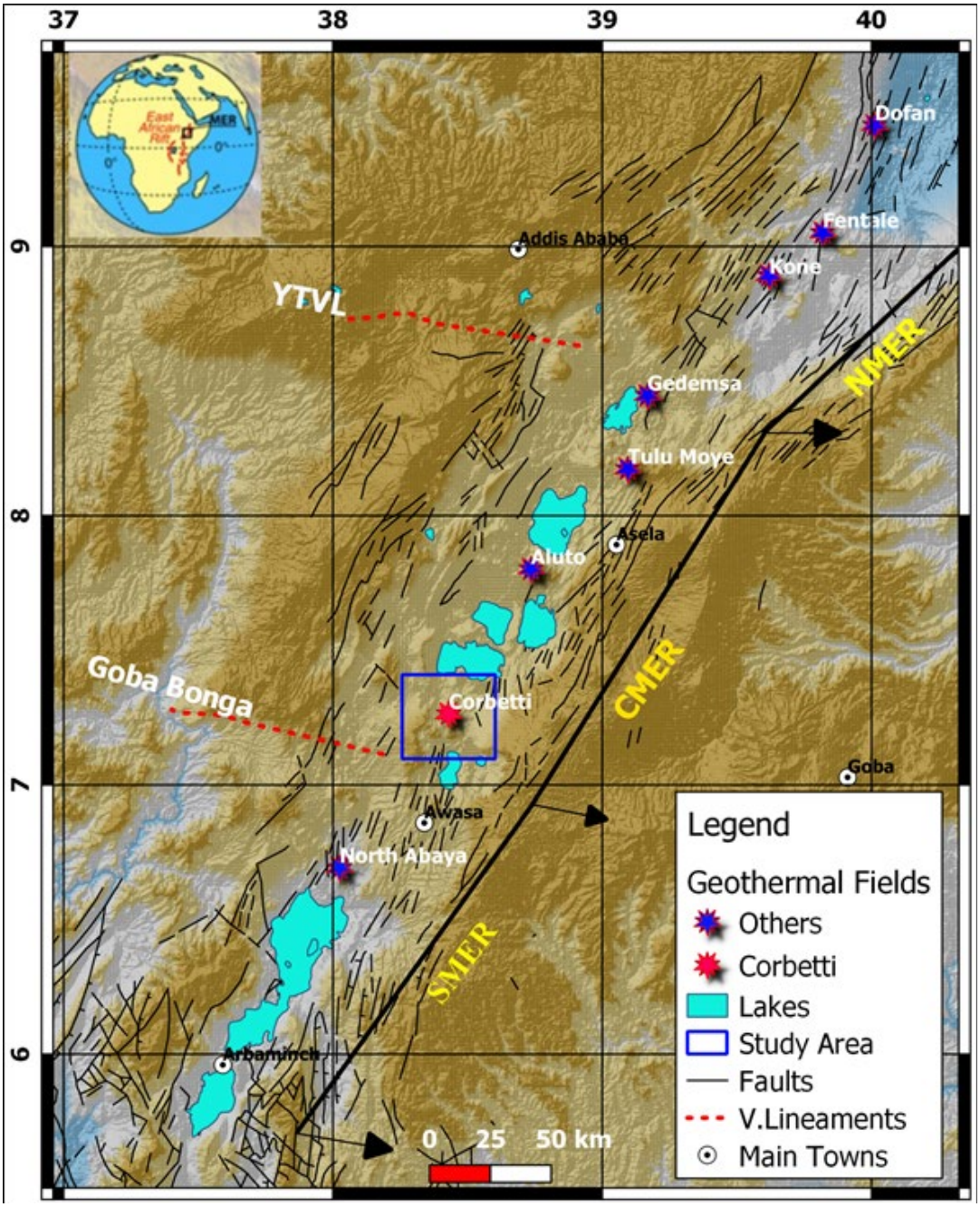

Figure 1: Location map of the geothermal prospect areas within the Ethiopian Rift Valley, Faults extracted from geological map of Ethiopia superimposed on GEBCO DEM (https://download.gebco.net/).

Geophysical surveys can be utilized at a wide range of scales, ranging from regional tectonic studies and sub-regional hydrocarbon, geothermal exploration and mineral exploration surveys to local engineering and environmental problems [22-29]. From the geological and hydrological points of view geothermal systems are very complex, thus a combination of techniques should therefore be employed to characterize the geothermal systems accurately [30, 31]. Thus in this paper integrated geophysical (gravity, magnetic and electrical resistivity) investigations are considered. The study stems from the necessity to collect new magnetic data that fills the missing magnetic data coverage over the volcano in order to make an effective use of geophysics for geothermal resource potential assessment tasks. The gravity method is used in mapping regional geological structures at large scale. The magnetic and the gravity methods are known to complement each other and therefore the magnetic method is also used in mapping the major lithological and structural units residing in the study area. The deep electrical sounding surveys would establish the vertical stratification of the geoelectric layers of the area. The investigations are made to possibly identi-

fy and locate subsurface geological structures associated with hydrothermally altered volcanic lying within their unaltered equivalents residing at the Corbetti Caldera. The outcome of the study may provide vital information to decide on the possibility of extending the geophysical investigations considered here for the assessment of the geothermal potential of the central MER volcanoes of Corbetti caldera complex.

Geological Setting of the Study Area

The Central MER extends from Lake Koka through the lakes region to Lake Awasa, with border faults trending in the NE-SW direction and the age of onset of extension in the CMER is still debated. The age of onset of faulting estimate to be 8.3–9.7 Ma with earliest syn-rift volcanics at □8 Ma, whereas estimate the onset of extension and initial volcanism to be 5–6 Ma [32-36]. Major rift-bound silicic centers such as Aluto, Bora, Corbetti, Gademsa, Gademotta, and Shalla, located along the rift floor of the central sector of the Main Ethiopian Rift (Figure. 1), were active during the Pleistocene, in addition to basaltic fissural eruptions of the Wonji Group [37-39].

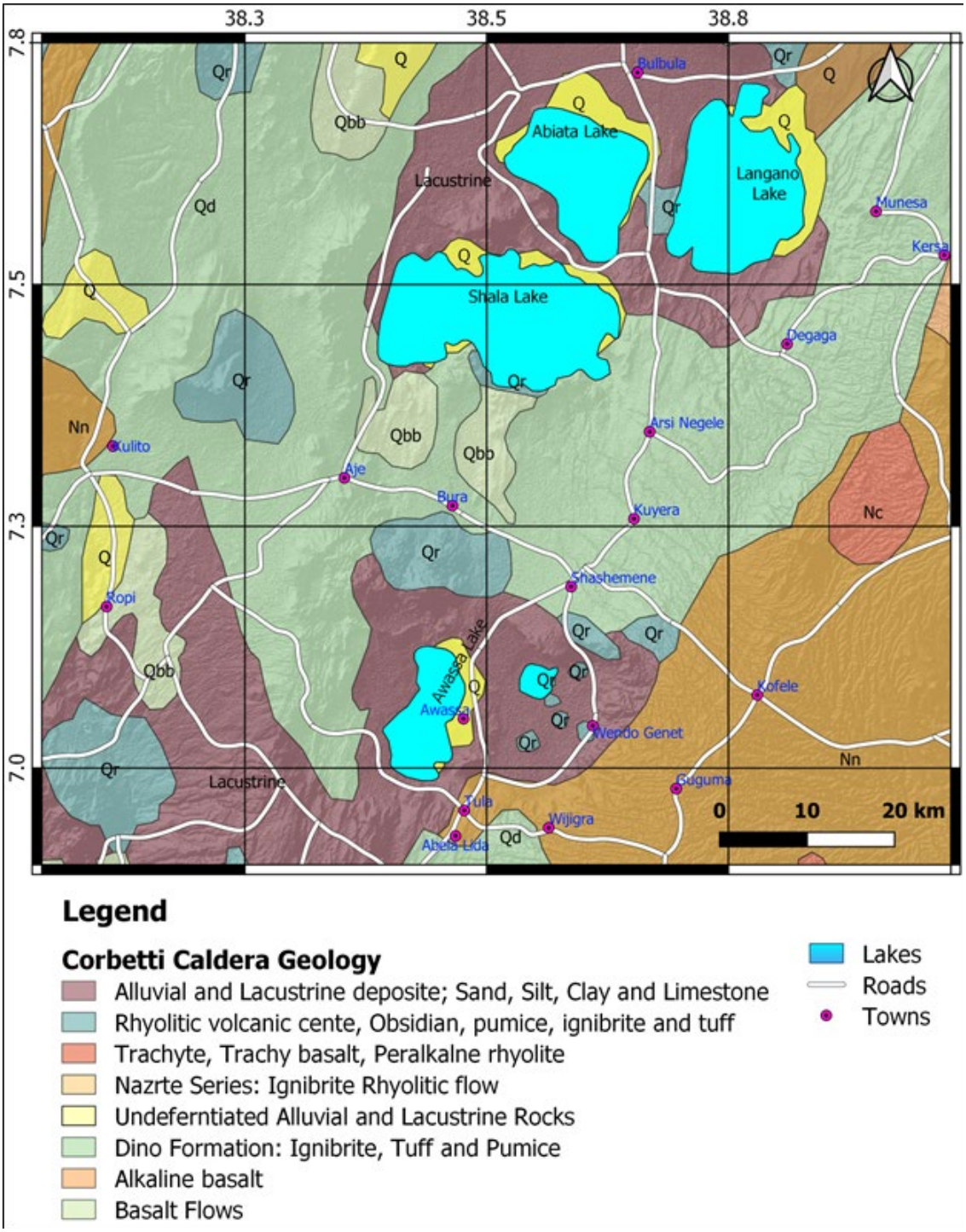

Figure 2: Geological Map of Central MER modified from Geological Map of Ethiopia 1:2,000,000 [40].

Post caldera activity around the Corbetti area is represented with the birth of three recent peralkaline volcanoes (Urji, Chebbi and Danshe). Based on geological and geochemical evidences, the evolution of the Corbetti volcano is determined to be associated with extensive fractional crystallization of parent mantle-derived basaltic magma occurring in a huge shallow level magma chamber and fumaroles, steaming and warm grounds are some of the hydrothermal manifestations in the Corbetti Caldera [41-43]. As to the geological compositions, it is within recent volcano tectonic activities on Wonji Fault Belt, mainly composed of per alkali-silicic products, rhyolite flows, obsidians, pumice, ashes, ignimbrites and the same nature of basaltic lava flows and scoria. There are pre and post caldera sediments and recent alluvium. All volcanic formation indicates starting from early formation of the caldera to the plio-pleistocene activities which are characteristics of the MER [44-46]. Urji, Chebbi and Danshe volcanoes are formed of pyroclastics which are represented by pumice falls; on the eastern side of Urji some obsidian interbedded with pumice outcrops. The difference between the three volcanoes is the amount of very recent obsidian lava flows which cover the pyroclastics of Chebbi [47]. There are many occurrences of fumaroles (steam vents) and hot ground (hot springs) in several places within the caldera. In general most of the hydrothermal manifestations are associated with recent volcanological fractures such as eruption centers, craters and caldera rims, controlled by structural features (faults, fissures, joints and contact zone). Hydrothermal manifestations i.e., altered ground with fumarolic activities are associated with fissures, craters, faults and caldera rims, where tectonic structures give major access for hydrothermal fluids [48]. Corbetti is a silicic volcanic system similar to Alutu volcano, except for it's being a well-developed resurgent cauldron system. The -caldera-forming volcano developed on terrain made up of late Tertiary ignimbrites. Later ignimbrites, which led to the collapse of the caldera, form the present rift floor surface in the area and the flanks of the caldera that are still intact. On the volcanic edifices situated inside the caldera, fissures oriented in the E-W direction cross, NNE-SSW trending regional rift forming faults [49-51]. The NNE-SSW trending regional rift forming faults are also observed on Southern MER [52-53].

Geophysical Datasets and Processing

In this study about 230 observed gravity and 56 electrical resistivity (VES) data are obtained from the Geological Survey of Ethiopia and more than 220 primary magnetic data are generated in the Corbetti Caldera complex (Fig 3) [54].

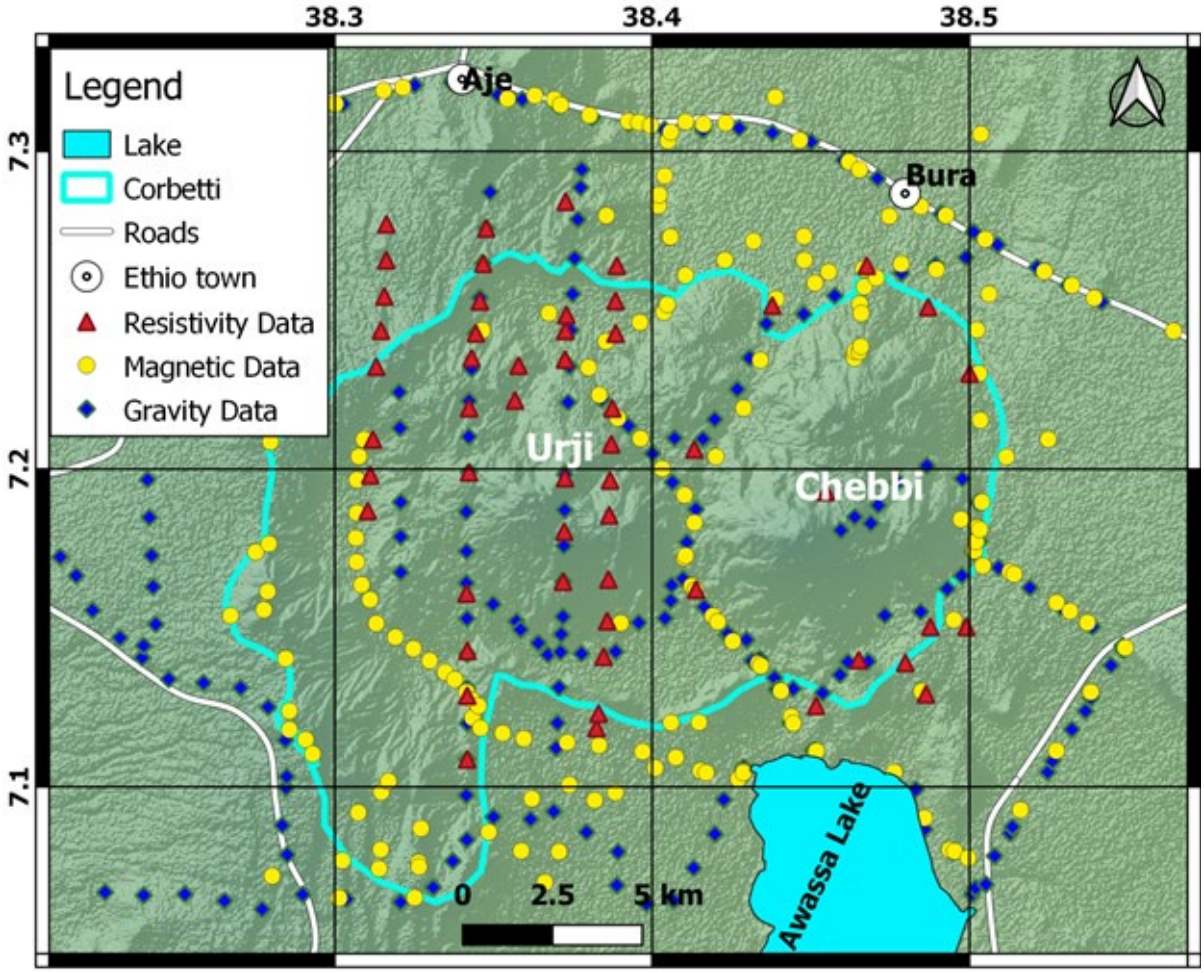

Figure 3: Location plots of Gravity, Magnetic and Electrical data point plotted on SRTM DEM.

The theoretical gravity, g at latitude ϕ, has been calculated using the 1967 gravity formula. A total of 230 observations are employed and were treated by a homogeneous reference to the IGSN 71 datum [55, 56]. Positions (latitude and longitude) and elevations of the gravity stations are determined by GPS (Global Positioning System) and altimeter measurements. A uniform reduction density of 2.67g/cm3 is used to compute the Bouguer anomalies and the computed Bouguer anomaly corresponds to complete Bouguer anomaly for all stations [57]. The complete Bouguer anomaly map represents the regional gravity anomaly of the study area of interests. Map presentation and processing, including the preparation of upward continued map from the complete Bouguer anomaly map, and separation of residual components from regional performed by reducing (removing) upward continued map from the regional gravity anomaly map using Geosoft Oasis Montaj 8.4v software [58]. The instrument used to collect the magnetic data is a proton precision magnetometer (IGS2) which measures the total intensity of the earth's magnetic field. Total field magnetic data were collected over random points and covering most of the areas over which the gravity and electrical VES were obtained as a secondary data from EGS. A total of about 220 data points were gathered with a station spacing of 500-1000 m. These data were then corrected for diurnal variations and unexpected data readings were removed from close examination of the data set. The magnetic anomaly is presented as total and residual magnetic anomaly, analytical signal anomaly and edge detection with source depth estimation map of the area.

Methodology

Interpretations and analysis of gravity data are carried out on free air and a complete Bouguer gravity anomaly map of the study area. The maps were produced with a grid spacing of 72.0m x 72.0m (Fig 4B&5).

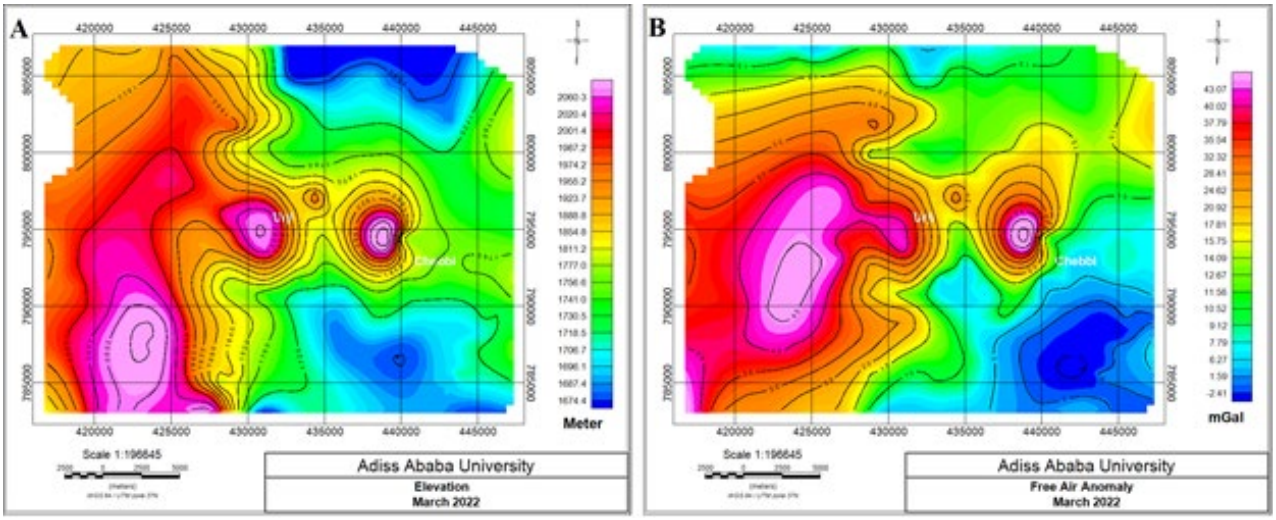

Figure 4: (A) Topographic maps, (B) Free-Air anomaly of Corbetti Caldera and its surroundings

The free air effect is simply the gravitational change caused by a difference in elevation between stations. The free air anomaly map (Fig 4B) shows a strong correlation with local topographic map (Fig 4A), this shows the reliability of the gravity data collected on the area [59-61]. The Free-air anomaly map shows its maximum, about 45mgal and its minimum -2mgal in the study area of interest, i.e., the Chebbi and Urji volcanoes are the highest elevated areas of Corbetti caldera which is about 2100m.s.l and the volcanoes are associated with maximum Free-air anomaly which is about 45mgal.

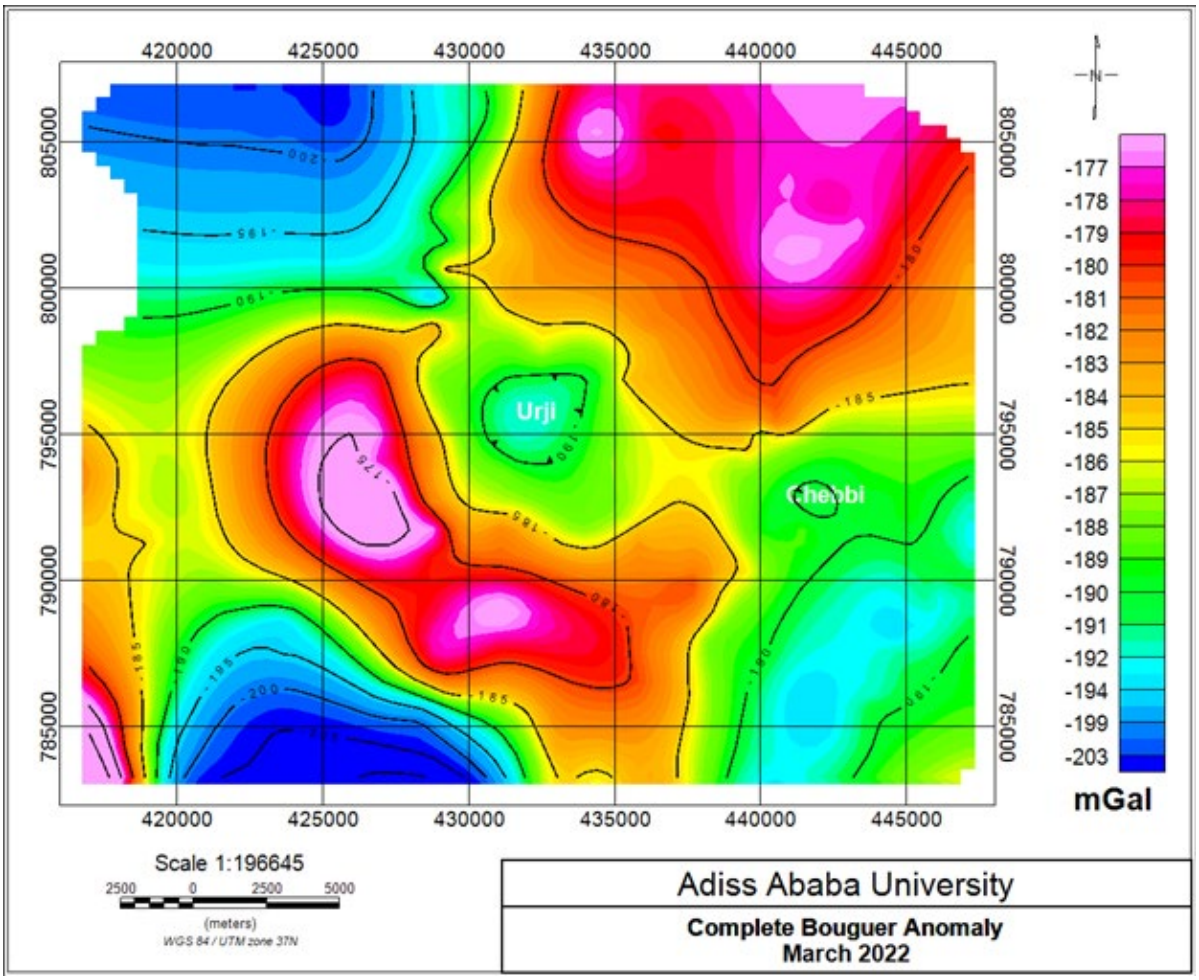

Figure 5: Complete Bouguer Anomalies of Corbetti Caldera and its surroundings.

Referring to the complete Bouguer gravity anomaly map (Fig 5), which correlate with only lateral variations in density of the upper crust, the magnitude of the Bouguer gravity anomaly varies from minimum of (-217mgal) to the maximum of (-190mgal) in the vicinity of the study area, and the anomaly map in general shows different contrasting zones, a circular low Bouguer gravity anomaly which is about (-200mgal) having a steep gradient located at the center of the Bouguer anomaly map has outlined the geologically inferred Corbetti caldera.

Gravity Anomaly Separation

Upward continuation can be used to separate a regional gravity anomaly resulting from deep sources from the observed gravity and it is an effective technique to estimate the regional gravity [62-64]. The upward continuation can be formulated as (R J Blakely, 1995) shown in (Eq.1) below:

$$F[U_u]=F[U]\times e^{-\Delta z.k} \quad (1)$$

Where F[U], $F[U_u]$ is the Fourier transform of the potential field U, upward continued field U_u, $\Delta z>0$ is elevation difference, and $k=\sqrt{(k_x^2+k_y^2)}$ is the radial wave number. The transform field is then computed by taking the inverse Fourier transform of $F[U_u]$.

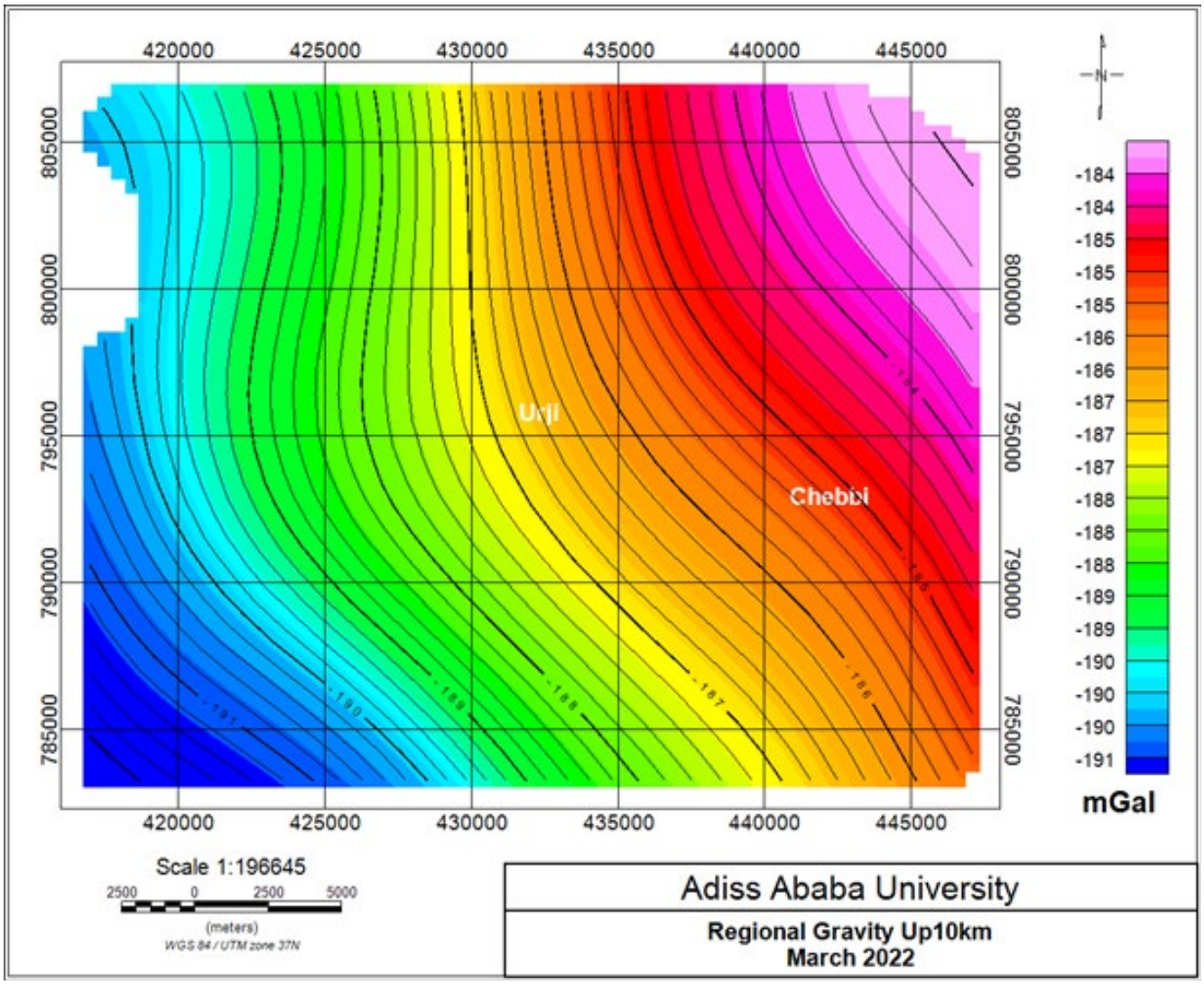

Figure 6: Regional gravity anomalies of the study area computed by upward continuation filter. Contour interval: 0.2mGal.

The optimal upward continuation height 10km is selected for the regional gravity anomaly field estimation by comparing and contrasting various heights depending on the target of investigations. Since the target depth of the geothermal prospect is approximately undulating 3km-4km, the data is upward continued at 10km to remove the short wavelength anomalies. It is possible to focus on sources situated at a depth greater than(z)(2), if a potential field is upward continued to a certain heightz , [65-67].

By removing the regional gravity anomaly (Fig 6) from the complete Bouguer gravity anomaly (Fig 5), the residual gravity anomaly of the area is computed (Fig 8).

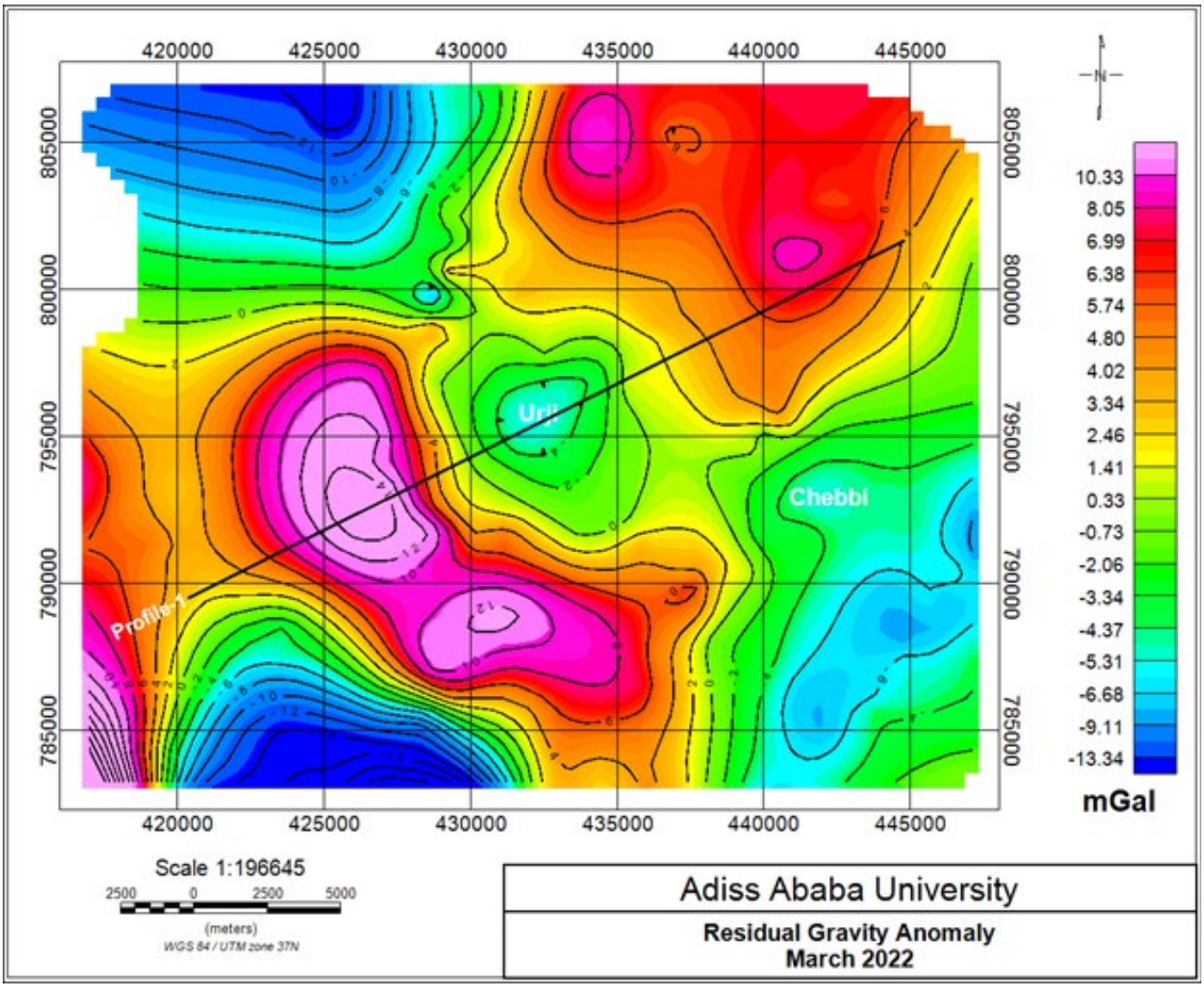

Figure 8: Residual gravity anomalies of the Corbetti Caldera and its surroundings.

The residual Bouguer gravity anomaly map (Fig 8), shows that the gravity anomaly of the study area varies locally from -14mgal up to 12mgal. Local positive and small negative gravity anomalies are observed in the residual map, which is related to denser mass intrusion and low density materials. Referring to the residual Bouguer gravity anomaly map (Fig 8), a circular negative gravity anomaly located at the center of the anomaly map outlined as the Corbetti Caldera and the sharp gradient of the residual anomaly at this region outlined as the Corbetti Caldera rim.

Total Magnetic Field Intensity

The total magnetic field intensity map shown in (Fig 10), is the regional magnetic anomaly map of the study area is prepared from the diurnally corrected magnetic data in which field intensity values lie between 34600nT-35400nT (Fig 10), the presence of prominent high anomalous features are observed NW-SE directions whereas the lower anomaly is confined in NE and SW part of the area.

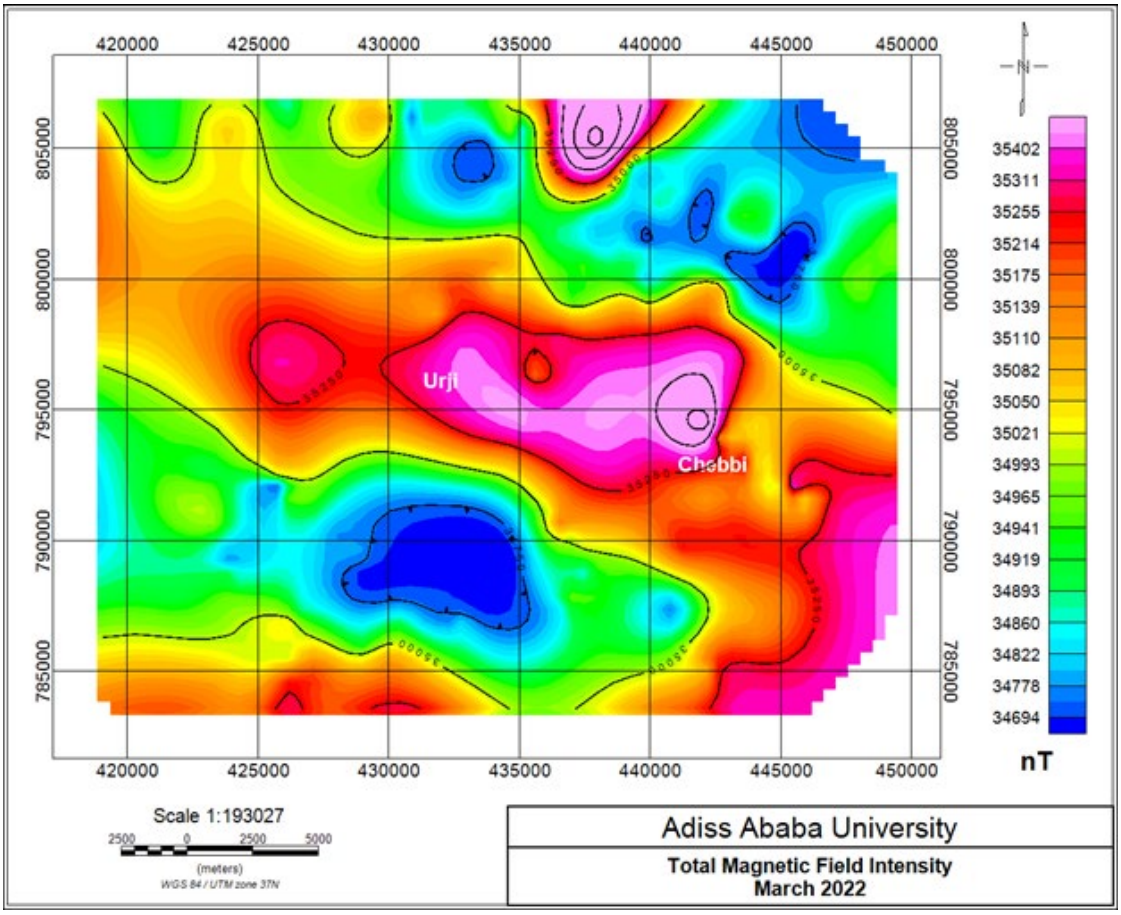

Figure 9: The total magnetic field intensity map of Corbetti Caldera and its surroundings

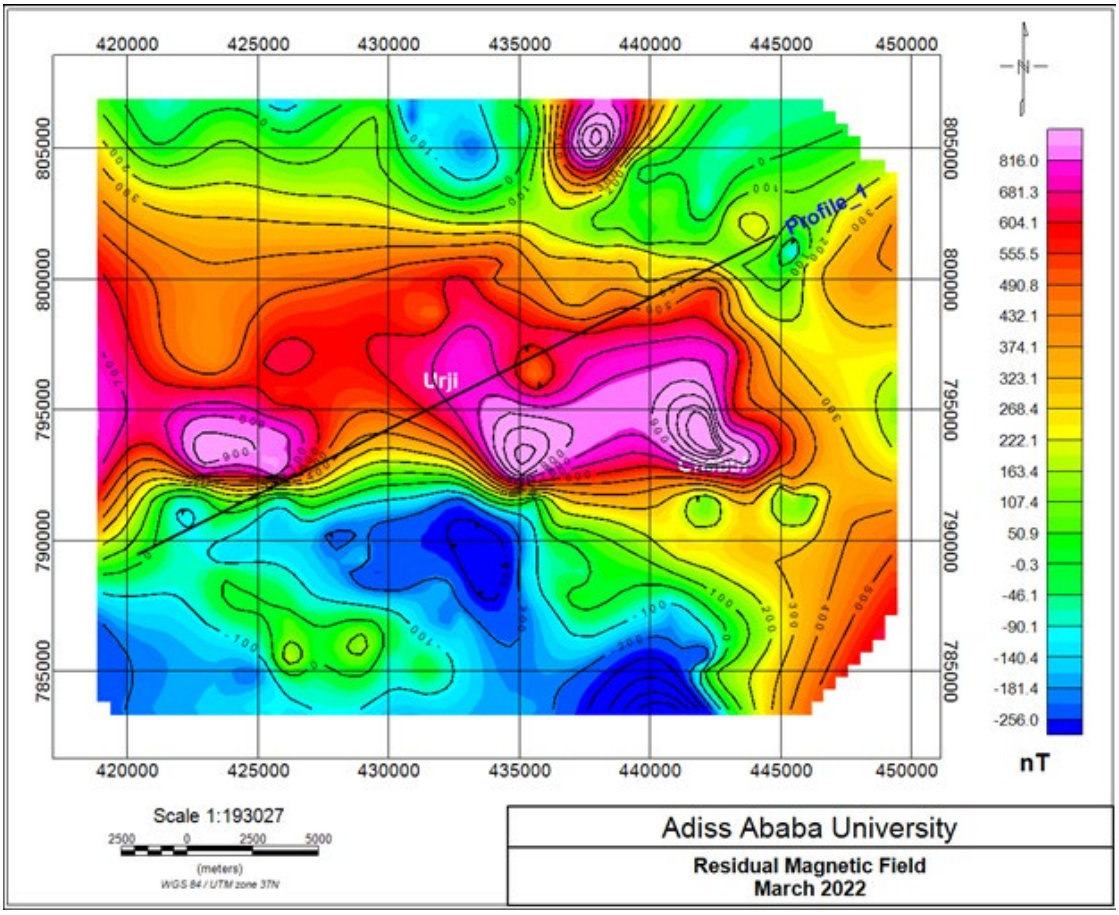

Figure 10: The Magnetic Anomaly Map of the Corbetti Caldera and its surroundings.

The magnetic anomaly map (Fig 10) reflects the magnetic effects of subsurface rocks whose susceptibility varies laterally from -250nT-90nT. The magnetic anomaly map almost coincides with the total magnetic field intensity map shown in (Fig 9), reflecting the low anomaly of northern and southern parts of the area separated by the wider NW-SE high anomaly trends traversed by the Urji and Chebbi Volcanoes.

Analytical Signal

Amplitude of the analytic signal can be defined as the square root of the squared sum of the vertical and the horizontal derivatives of the magnetic field (Eq. 2).

$$As|(x,y)|=\sqrt{(\partial A/\partial x)^2+(\partial A/\partial y)^2+(\partial A/\partial z)^2} \quad (2)$$

Where As is the amplitude and M is magnitude of the total magnetic field.

The analytical signal (Fig 11) is formed through a combination of horizontal and vertical gradients of a magnetic anomaly and the method is very useful for delineating magnetic sources. The amplitude of a simple analytic signal peaks over magnetic contacts [68]. Therefore, the procedure can also be used to find location of horizontal contacts and depths of magnetic contacts. The analytic signal has a form over causative bodies that depend on the locations of the bodies but not their directions of magnetization.

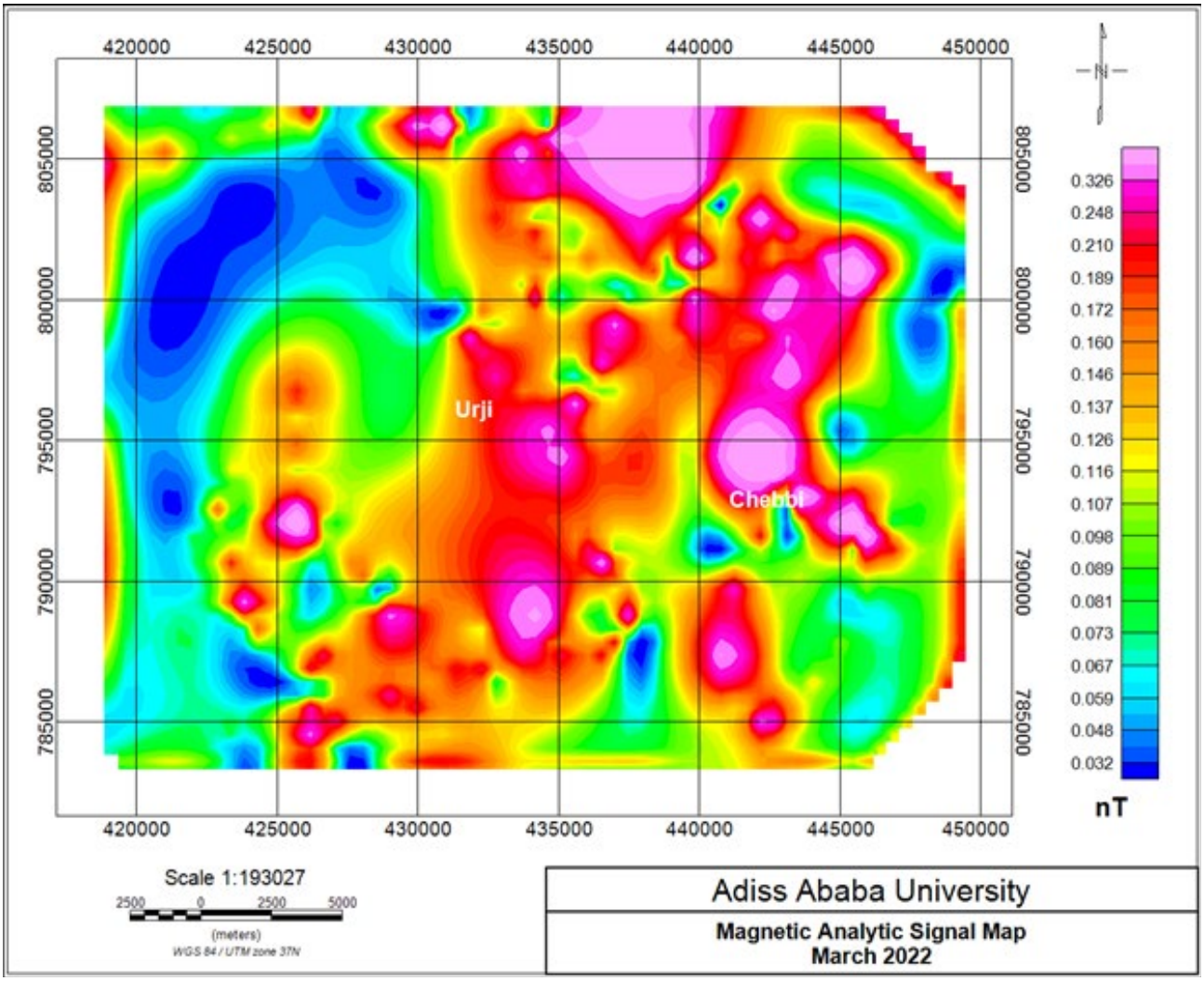

Figure 11: Analytic signal anomalies of Corbetti Caldera and its surrounding.

Volcano Tectonic Lineament Detection Using Tilt Angle Method

Developed the tilt angle method computed as the arctangent of ratio of the first vertical derivative to the first horizontal derivatives of the gravity field shown in (Eq. 3) below [69].

$$\theta = \tan^{-1}(\partial M/\partial z)/\sqrt{((\partial M/\partial x)^2+(\partial M/\partial y)^2} \quad (3)$$

Where θ is Tilt angle Filter, M is the gravity or magnetic field and $\partial M/\partial z$,$\partial M/\partial x$ and $\partial M/\partial y$ are the first derivatives of the field M in the x, y and z directions.

Used tilt angle computed from analytic signals to estimate the source location parameters of simple gravity bodies. Thus in this paper the tilt (Fig. 12) angle is computed from the Analytic Signal Map (Fig. 11).

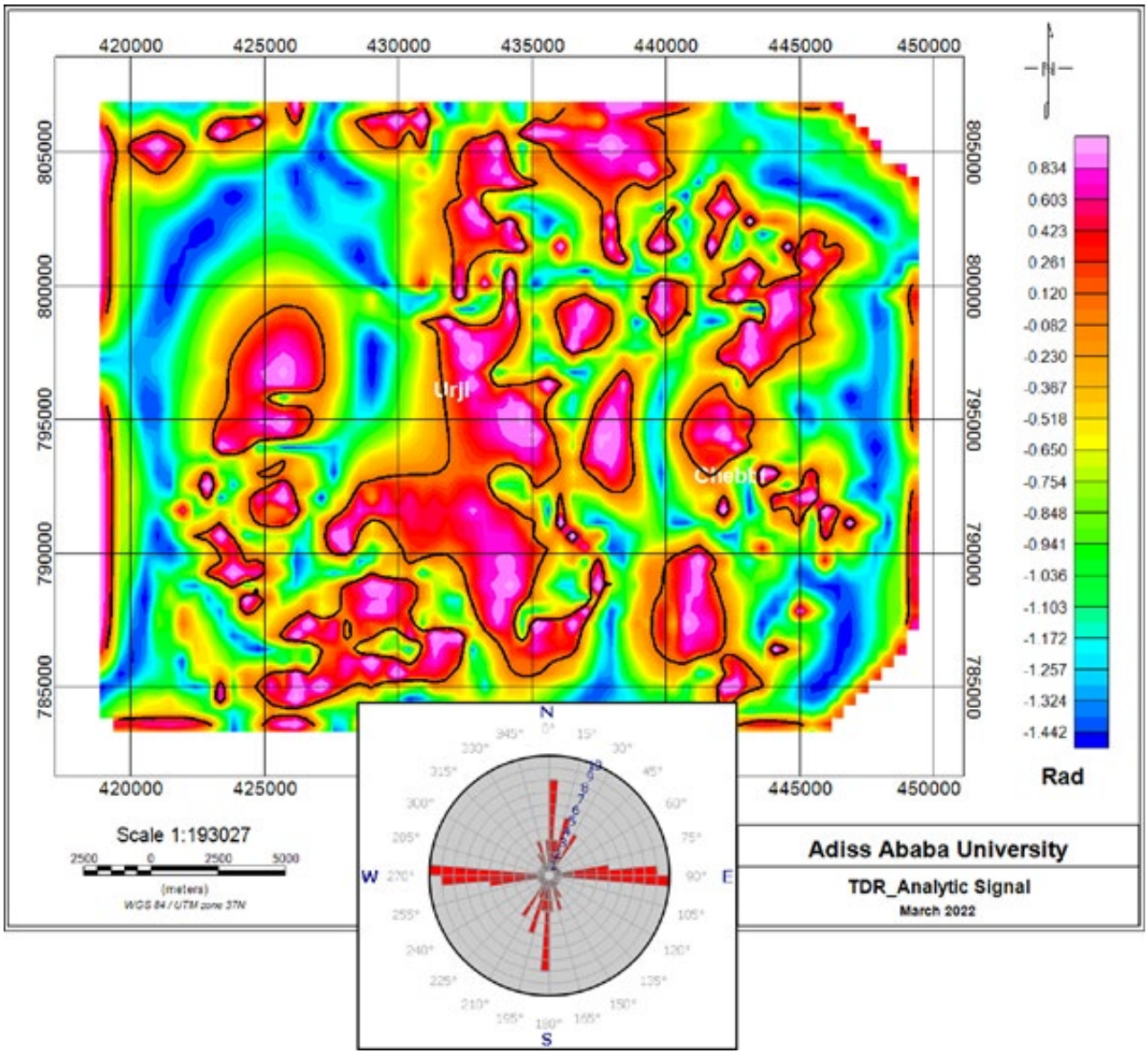

Figure 12: Tilt angle map generated from Analytic Signal: Rose diagram highlighting the orientations of the main trend

The tilt angle method is effective in discriminating signal for both shallow and intermediate sources and its amplitudes are restricted to values between $-\pi/2$ and $+\pi/2$ according to the nature of the arctangent trigonometric function and respond to a large dynamic range of amplitudes for anomalous sources at the different depths [70, 71]. The directional analysis performed on the extracted Volcano tectonic lineaments (Fig 12) shows the E-W, N-S and NE-SW trending lineaments.

Source Depth Estimation

The depth to the top of Volcanic Tectonic Lineaments (VTL) can be computed corresponds to the distance between 0^o and 450^o adaptive tilt angle values ($h=z\_(c\ ))$; as described by as shown in (Eq. 4) below;

$$\theta=\tan^{-1}[h/Z_c] \quad (4)$$

Where h the horizontal distance from the source is, θ tilt angle and z_c is the depth to the contact or volcanic lineaments.

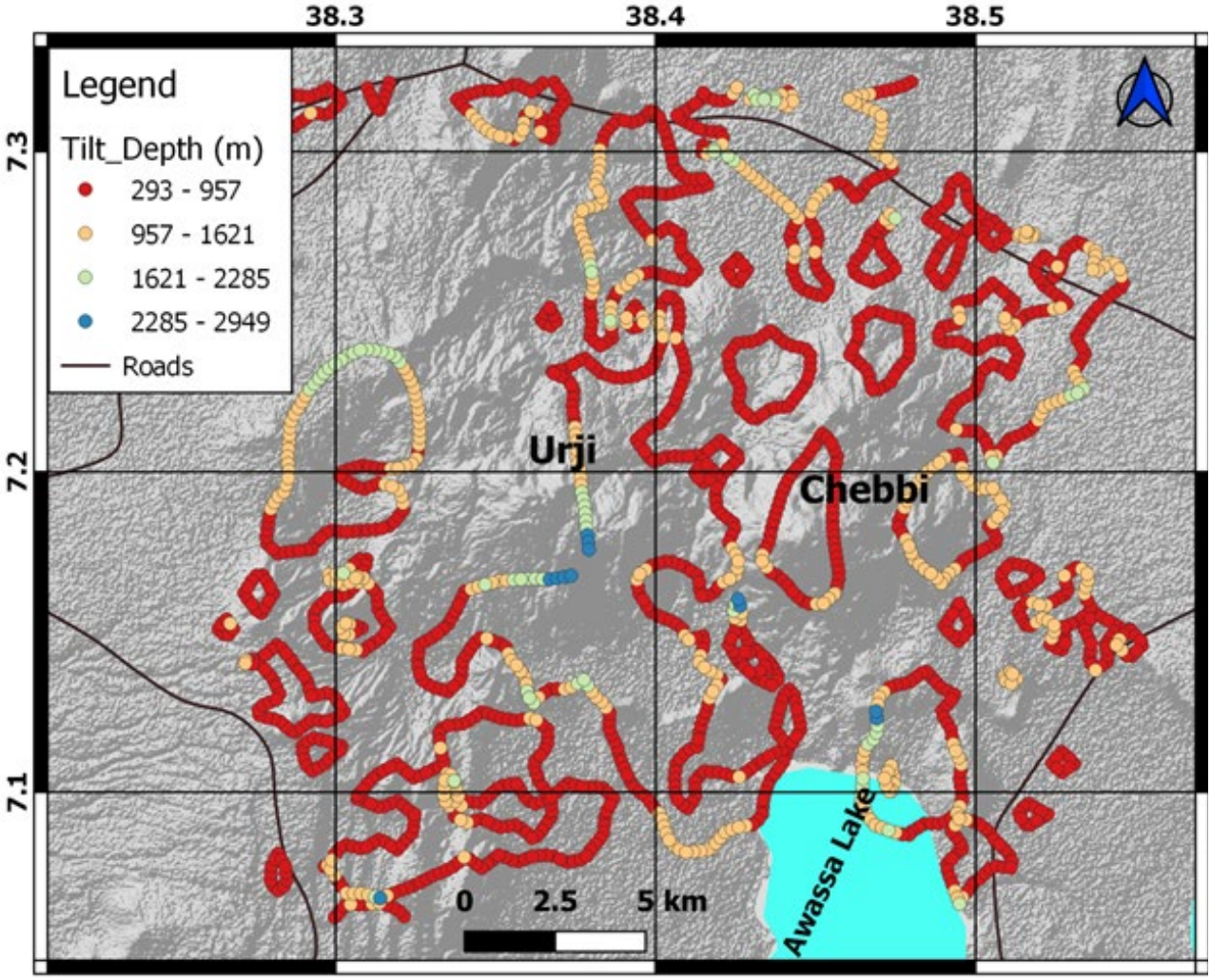

Figure 13: Top of VTL Depth extracted from tilt map prepared from analytic signal displayed on SRTM-DEM hill shade.

The depth estimation to the top of the volcanic lineament from tilt angle ranges from 293m to 2949m (Fig 13). Relatively deeper sources are observed on Urji Volcano where shallower and intermediate source depth is observed on Chebbi Volcano.

Constrained Gravity and Magnetic 2D-Modeling

The forward modeling of the gravity and magnetic field has been done with GM-SYS 5.01.10 software which is an extension of Geosoft Oasis Montaj and it has a paramount importance to interpret the gravity and magnetic field quantitatively and the profile line is generally aligned in the general direction of the axial portions of the Main Ethiopian Rift, that is, from southwest toward north east as shown in the residual Bouguer gravity and magnetic anomaly maps (Fig 8&11). The model shown in (Fig 14) reflects a variety of structures with different lithology. The model produces a suitable fit with the observed gravity data with (RMS) of 3.22mgal. The densities of the lithology shown in the gravity model exhibit a variation of approximately 10 – 15 %. The magnetic and gravity fields have identical profile lines with an assumption that comparing and contrasting the two potential fields may give a better resolution of the geological and structural features of the Corbetti caldera along the profile. The susceptibility of the lithology shown in the magnetic model exhibits a variation of approximately 10 – 15 %.

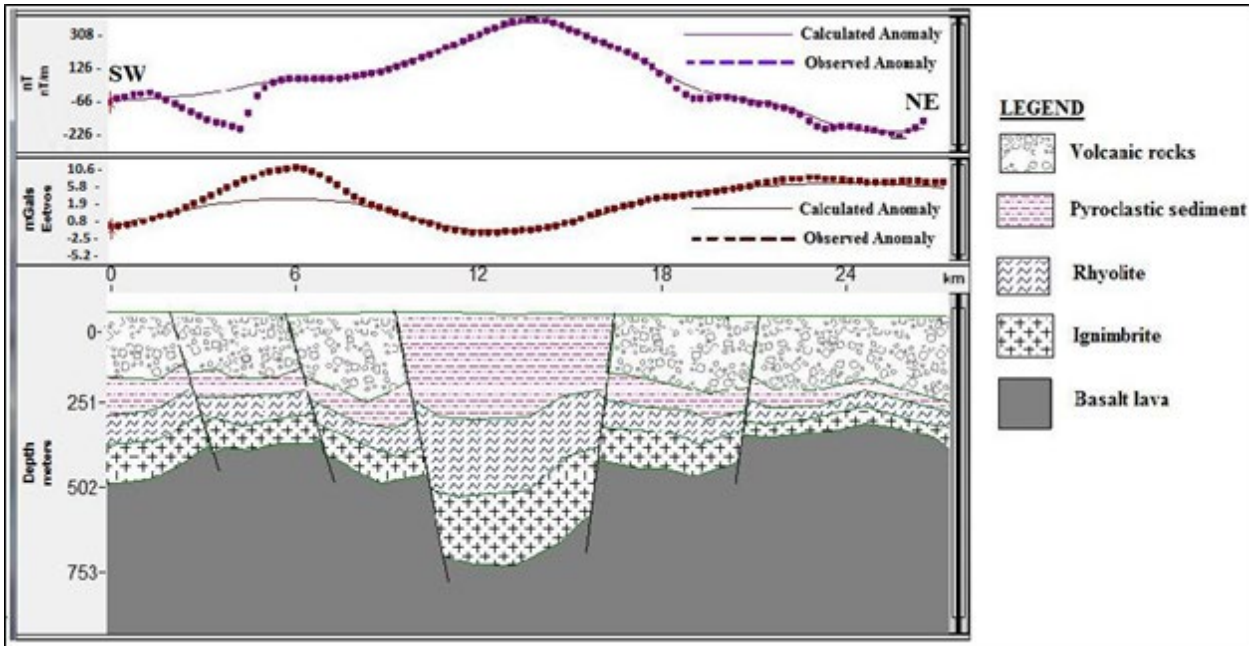

Figure 14: The Gravity and magnetic field modeling along the profile-1.

Shclumberger Apparent Resistivity Plots

The Shclumberger apparent resistivity map for AB/2=1810m and AB/2=2700m (Fig 15A&B) are prepared using Geosoft Oasis Montaj for qualitative interpretations of the variation of the apparent resistivity of the study area at a shallow depth [72, 73].

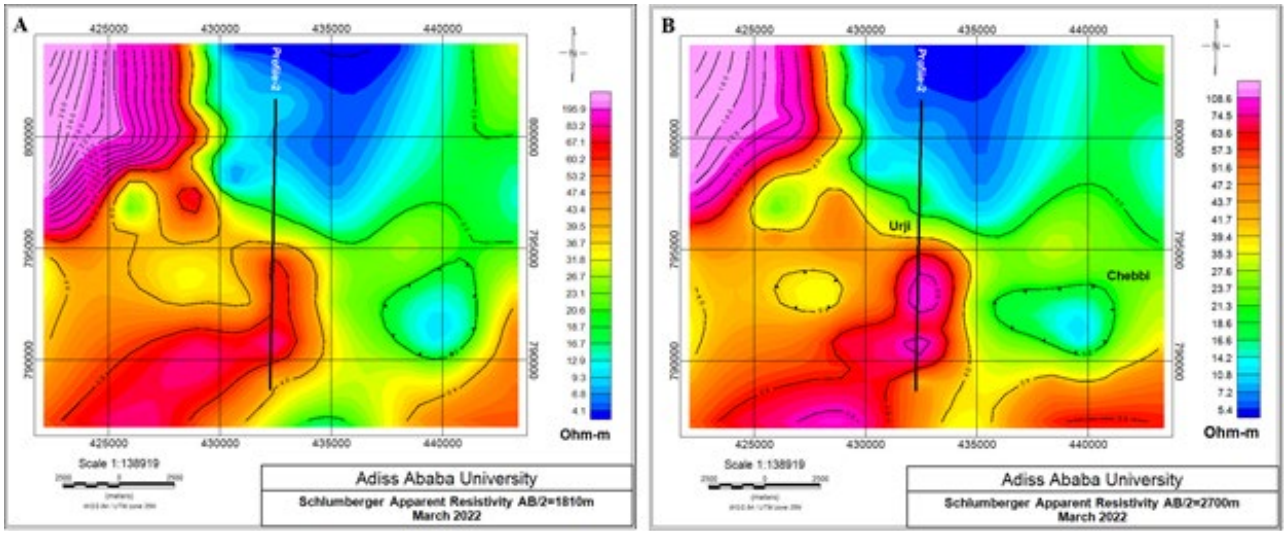

Figure 15: The Schlumberger apparent resistivity map: (A) AB/2=1810m and (B) AB/2=2700m

Interpreted Curve and Geoelectric Section along Profile-2

There are twelve VES data points along the profile and each VES point was inverted using IP2WIN. The inverted curve has 5-7 geoelectric layers with minimum error 4-9%.

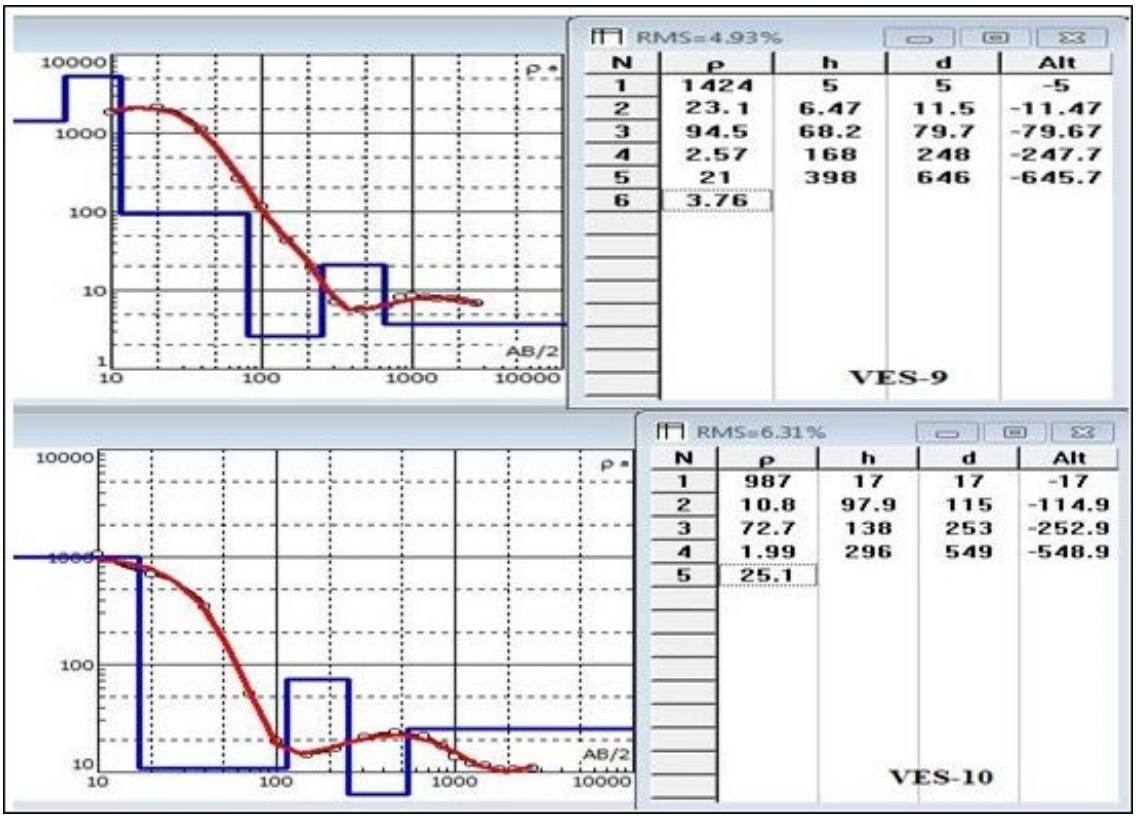

Figure 16: Sample, VES-9 and VES-10, interpreted curves

Both the resistivity curve (Fig 16), shows higher resistivity on average more than 1000Ω.m found at the top layer and a gradual decrease of resistivity reaching to 3Ω.m as the depth increases. These two curves are selected as a sample, out of the twelve curves in which all the curves somehow exhibit similar properties.

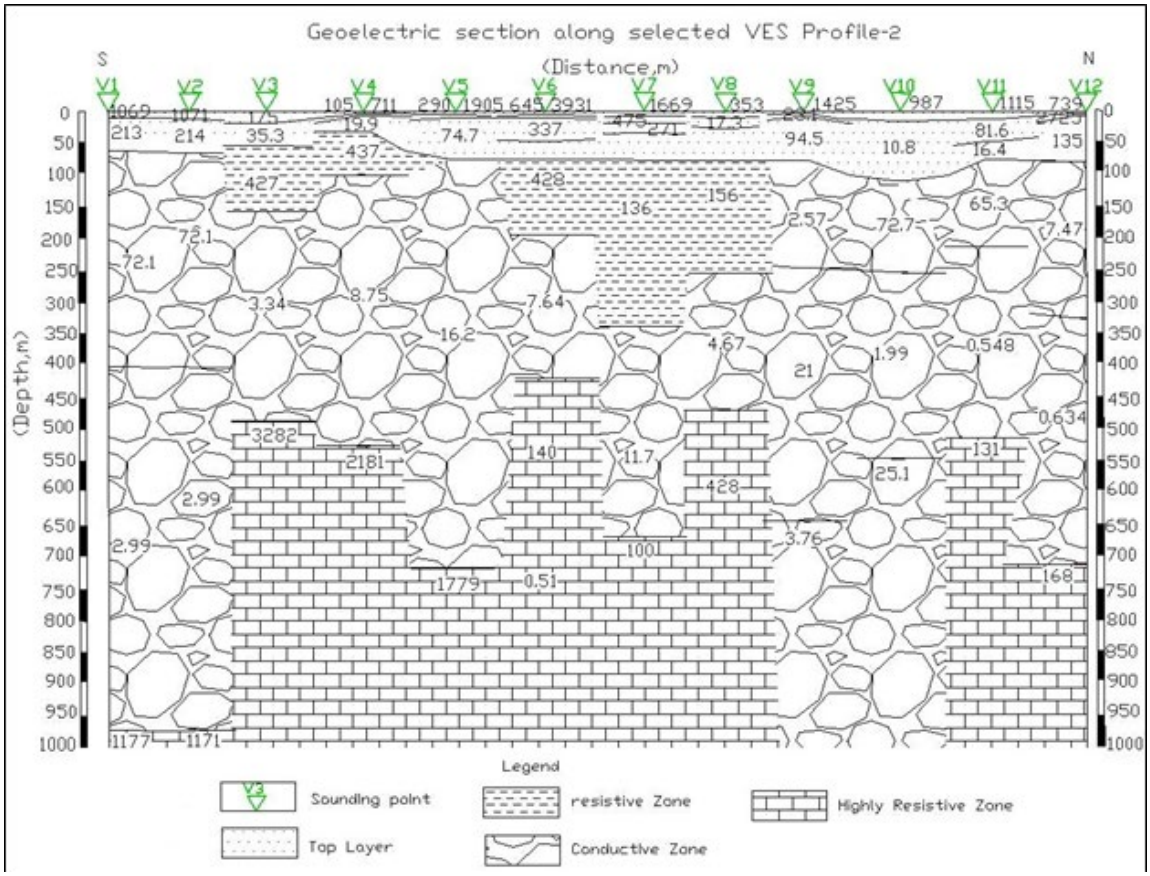

Figure 17: The Geoelectric section along profile-2

The Geoelectric section shown in (Fig. 17) is prepared from the interpreted curves using AutoCad-07. The Geoelectric section generally separated into three parts, the top layer in which the resistivity varies from 80Ω.m - 2750Ω.m, having thickness of 50m – 100m, discontinuous Resistive zone 136 Ω.m - 437 Ω.m at the center of a section with thickness between 100m-150m and Conductive zone with resistivity ranging 0.548 Ω.m to 72 Ω.m, with variable thickness 200m up to 800m.

Result and Discussion

The Corbetti caldera having elevated volcanic complexes such as Chebbi and Urji is a nested caldera within the Awassa caldera. The region as it is shown in the topographic map (Fig 4A), is delineated as higher elevation between 1900 and 2100 meters and is located in the central parts of the caldera where Chebbi and Urji volcanic complexes are located. Local depressions designated by lower elevation values of (1600-1750) meters are shown in the North eastern and south eastern parts of the study area. Close inspection of the geological map (Fig. 2) of the region reveals that this low elevated region is dominated by major semi-regional faults and collapsed structures which are associated with the eastern escarpment of the rift. The Bouguer gravity anomaly (Fig. 5) varies from minimum of -217mGal to a maximum of -190mGal in the vicinity of the study area. The Bouguer gravity anomaly acquires a maximum value to the NE and SW of the Corbetti caldera. The NE part of the Corbetti caldera generally gained a high gravity anomaly value of (-192 mgal to -187 mgal). The SE part of the caldera which appear like a curve running from SE to NW below the caldera acquire a high gravity anomaly value of -193mgal to -190mgal. These may be interpreted as the effect of high density materials coming from the mantle during the formation of the Corbetti caldera. The SW and NW of the Corbetti caldera shows the minimum value of the gravity anomaly (Fig. 5) of -207 mGal to -217 mGal, which could be interpreted as a crustal anomaly that is generated by low density materials. In general Corbetti caldera is associated with a high gravity field with slight modifications by the product of Chebbi and Urji volcanoes which relatively exhibit low gravity anomaly. This is due to the fact that the Corbetti caldera consists of mantle materials of large denser intrusion which comes to the crust during the volcanic activities. Previous seismic observations and Bouguer gravity of the central MER suggest that the density of the upper crust above 5 km is 2,400–2,470 kgm−3 b.s.l. and □2,670 kgm−3 below 5 km b.s.l. which implies an addition of material with higher mass density than that of surrounding rocks.

Referring to the upward continued gravity anomaly map (Figure 6), the gravity anomaly shows a continuous increment from the SW to NE in the vicinity of the study area. The upward continued gravity anomaly map shows the gravity anomaly of deep Earth origin. The continuous gravity anomaly increment without interruption from SW to NE is found in the direction along the axial portion of the Main Ethiopia Rift (MER) which could be interpreted as, decrease of crustal thickness along the axial portion of the Main Ethiopia Rift (MER). The denser mantle materials approaching nearer and nearer to the surface from SW to the NE has an enormous effect on the gravity anomaly increment along this direction. Urji and Chebbi volcano acquires a local negative anomaly (Fig 7) about -8mGal to -6mGal, which might be driven by low density material such as hydrothermal fluids and enclosed by hydrothermal vents at the volcanic centers. Referring to the geological map (Fig. 2), compared to other parts of the caldera, Urji and Chebbi are covered with thicker low density formation (pumice). Urji and Chebbi volcano explosive eruptions generate widespread and thicker pumice fall deposits in the area. A very high local gravity anomaly which is about 9mgal to12 mgal in the study area was interpreted as a dense intrusion driven from the mantle materials to the crust by volcanic activity. The NW and SW parts of the Corbetti caldera show high negative anomaly which is about -12 mgal to -14 mgal. A geological structure (graben) is assumed to be the causes of the local low gravity (low density) anomaly which could be a thick in fill of lake sediments, pyroclastic deposits.

Referring to the total magnetic field intensity map (Fig. 9), in a region running from SE to NW in which the Chebbi and Urji volcano is presented, the regional magnetic field intensity shows a maximum value. This maximum total magnetic field intensity may be due to the existence of transversal E-W direction fissures. On the other hand the SW and NE parts of the Corbetti caldera shows very low total magnetic field intensity correspondingly maximum Bouguer gravity anomaly. These maximum peak gravity anomaly is interpreted as the effect the high density materials coming from the mantle during the formation of the nearby Corbetti caldera and post caldera activities. The very low total magnetic field intensity in this area may be interpreted as the thermal alteration of the magnetic minerals due to geothermal fluids in this region lowering the magnetic susceptibility values of any potential sources.

The analytic signal map of the Corbetti caldera (Fig 11) is produced from the total magnetic field anomaly map (Fig. 9). Close examination of the map confirms the existence of abnormal limiting (anomaly peaks). Medium anomaly peaks are observed over the Chebbi volcano and its surrounding and also to the south of the Urji volcano. The highest analytic signal anomaly peaks are shown on this map to the north of the Corbetti caldera rim, where the electrical resistivity slice section (Fig.15) map shows the lowest resistivity.

Referring to the gravity and magnetic model in (Fig.12), the top layer consisting of volcanic rock of density 2.57g/cm3 and magnetic susceptibility 0-50 nT. The thickness of this layer approximately varies from 140m to 220m, however, at the center of the caldera (in which the Urji volcano is nested, that is, filled with a pyroclastic sediments of density about 1.3 g/cm3 and a magnetic susceptibility range of 0.01 – 1595 nT), the thickness is estimated to an average of 330m. The residual Bouguer gravity anomaly map in (Fig. 7) clearly defines the Corbetti caldera with a circular negative anomaly and the rim of the caldera with sharp gradients of the anomaly. Therefore, the two middle faults in the gravity model indicate the caldera rim and the area between the two faults covered with thick pyroclastic deposit. The thin section which is overlaid by the volcanic rock at SW and NE of the caldera rim is pyroclastic sediments with approximate thickness of 80 -100m and average density of 2g/cm3. The layer underlain the pyroclastic sediments is a rhyolite of density 2.52g/cm3 and a magnetic susceptibility of 0.2nT -3595nT. A larger thickness varying in the Corbetti caldera is about 250 – 350m. A smaller

thickness of 70 – 100m is found to the SW and NE of the caldera. The overlaid ignimbrite rock has density value of 2.64g/cm3 and magnetic susceptibility 50nT with variable thickness of 100 – 300m. The basement is consists of basalt lava with a density value of 2.8g/cm3 and magnetic susceptibility value in the range 0.2nT -175nT. The volcano-tectonic lineaments (Fig. 12) unraveled by tilt angle shows trending in E-W, N-S and NE-SW direction, in agreement with the structural analysis performed by and lineaments extracted by Full Tensor Gravity anomalies of Southern MER. The depth estimated (Fig. 13) to the top of the volcanic lineament from tilt angle ranges from 293m to 2949m which is approximately equivalent to the depth to the top of the extracted lineaments using the same method in southern MER.

From the Schlumberger apparent resistivity map for AB/2=1810m and AB/2=2700m (Fig 13A&B) low resistivity anomaly follows the eastern and northern caldera rim, stretching north of the caldera towards Lake Shalla. Referring to the resistivity map AB/2=1810m, two areas are identified with a resistivity of 10Ω.m, that is, south and north of Chebbi and north of Urji. A close observation of the anomaly map i.e., south and north of Chebbi, some 10Ω.m resistivity closures is indicated within this zone in the caldera although the effect of topography and shallower resistivity structures have canceled this low resistivity anomaly. A low resistive zone located north of the caldera in which the topographic effect considered to be small and cover relatively larger area with 10Ω.m can be interpreted as a thermally altered zone associated with the intrusive heat of the Corbetti caldera by taking into consideration of the resistivity map of AB/2= 2700 we observe that the sequential decrease in a resistivity along the eastern parts of the caldera rim from 80Ω.m to 7Ω.m from south to the north which is similar in this way to the resistivity map AB/2=1810m. Since Lake Awassa is at higher elevation (1680m a.s.l) than Lake Shalla (1570m a.s.l), this may show that the local hydrological situation is such that ground water flow is from south to the north of the Corbetti Caldera thus the ground water interact with the intrusive heat of the Corbetti caldera may contribute to the sequential decrease of the resistivity from south to north along the eastern caldera rim, with supporting evidence of the presence of hot springs on the southern shore of Lake Shalla could mean a contribution from the Corbetti caldera to the hot fluid of the Shalla system and absence of the thermal features south of the Corbetti caldera is a clue to predict the hot water migrates from the caldera to Lake Shalla.

The geoelectric section shown in (Fig 15) is prepared from the interpreted curves using Auto Cad-07. The geoelectric section generally separated into three parts, i.e., the top layer in which its resistivity varies from 80Ω.m - 2750Ω.m, in which its thickness increases from 50m – 350m from Urji volcano to the northern parts of the caldera. Referring to the geologic map the Urji volcano approximately located under VES-4-VES-10 covered with thicker low density formation (pumice) up to 350m depth at the top layer and 50m – 100m thick under VES-1, VES-2, VES-3, VES -11 and VES-12 is lake sediments and alluvium. The middle conductive zone which acquires a very low resistivity from 0.56Ω.m - 75Ω.m with a variable thickness 200m - 900m, one of the reasons for resistivity to decrease is the increase in temperature, the other reason for the decrease of resistivity of rocks is the assemblage of conductive minerals due to alteration. The geoelectric section shown in (Fig 15), the bottom highly resistive zone in which its resistivity varies from 100Ω.m - 3290Ω.m having a variable thickness from 50m – 550m may be interpreted as Rhyolite and Basalt lava which is common in the area.

Conclusions

Corbetti caldera is associated with a high gravity field with slight modifications by the product of Chebi and Urji volcanoes which relatively exhibit low gravity in the vicinity of the study area. This is due to the fact that the Corbetti caldera consists of mantle materials of large denser intrusion which comes to the crust during the volcanic activities. The very high local as well as regional Bouguer gravity anomalies indicates the existence of intrusions beneath the caldera, in contrary those areas with very high gravity anomalies shows very low total magnetic field intensity, hence it seems that the intrusive bodies acts as a sources of heat in the vicinity of the area of interest i.e., due to the very high heat which is generated by the intrusion the rock which exhibit a magnetic property loses their magnetization. The local Bouguer gravity anomaly clearly defines the caldera with a circular gravity anomaly and the caldera rim with sharp gradient of the local gravity anomaly. The Schlumberger apparent resistivity map for AB/2=1810m and AB/2=2700m shows low resistivity anomaly follows the eastern and northern caldera rim, stretching north of the caldera towards Lake Shalla, this sequential decrease of the resistivity along the eastern parts of the caldera rim from 50Ω.m to 4Ω.m in the direction of south to north, with the absence of the thermal features south of the Corbetti caldera and hot springs on the southern shore of Lake Shalla is a clue to predict that the hot water migrates from the Corbetti caldera to Lake Shalla, i.e., the groundwater flows from Lake Awassa to Lake Shalla interacts with the intrusive heat of the Corrbetti caldera at the middle of the two Lakes thus, the hot fluid of the Shalla system could mean a contribution from the Corbetti caldera. The apparent resistivity pseudo sections and the true resistivity geoelectric sections show the presence middle thicker conductive zone which is associated with the increase in temperature and alteration. The magnetic and gravity data analysis results in the form of modeled sections show the presence of structures on survey lines and these structures are aligned in the general direction of rift (Southeast- Northwest direction). Even though the geophysical data used in this research is very restricted to the study area due to limitation of resources, based on the joint analysis of these geophysical methods and the dominant thermal manifestation toward the north of the Corbetti caldera which is to the south of Lake Shalla, the area has large scale geothermal potential for further development from center of caldera in which the Urji and Chebbi volcanoes are nested toward the southern shores of Lake Shalla.

Declarations

Authors' Contributions Statement

Bisrat Kebede: Conceived and designed the experiments; Performed the experiments; Analyzed and interpreted the data; Contributed reagents, materials, analysis tools or data; Wrote the paper.

Abera Alemu: Analyzed and interpreted the data; Contributed reagents, materials, analysis tools or data; Wrote the paper.

Hailemichael Kebede: Analyzed and interpreted the data; Contributed reagents, materials, analysis tools or data; Wrote the

paper.

Enatfenta Melaku: Contributed reagents, materials, analysis tools or data; wrote the paper.

Dejene Feyissa: Contributed reagents, materials, analysis tools or data; wrote the paper.

Guta Legesse: Contributed reagents, materials, analysis tools or data; wrote the paper.

Funding

This research did not receive any specific grant from funding agencies in the public, commercial, or not for profit sectors.

Conflict of interest /Competing Interest

The authors declare no conflict of interest.

Availability of Data and Material

The data that has been used is available on request

References

1. Abbate, E., & Sagri, M. (1980). Volcanites of Ethiopian and Somali Plateaus and major tectonic lines. Atti Convegni Lincei, 47, 219-227.
2. Abebe, T. (2000). Geological limitations of a geothermal system in a continental rift zone: example the Ethiopian rift valley. In Proceedings World Geothermal Congress, Kyushu-Tohoku, Japan, May.
3. Bellahsen, N., Faccenna, C., Funiciello, F., Daniel, J. M., & Jolivet, L. (2003). Why did Arabia separate from Africa? Insights from 3-D laboratory experiments. Earth and Planetary Science Letters, 216(3), 365-381.
4. Ebinger, C. J., Yemane, T., Harding, D. J., Tesfaye, S., Kelley, S., & Rex, D. C. (2000). Rift deflection, migration, and propagation: Linkage of the Ethiopian and Eastern rifts, Africa. Geological Society of America Bulletin, 112(2), 163-176.
5. G Ghebreab, W. (1998). Tectonics of the Red Sea region reassessed. Earth-Science Reviews, 45(1-2), 1-44.
6. Morley, C. K., Wescott, W. A., Stone, D. M., Harper, R. M., Wigger, S. T., & Karanja, F. M. (1992). Tectonic evolution of the northern Kenyan Rift. Journal of the Geological Society, 149(3), 333-348.
7. Burnside, N., Montcoudiol, N., Becker, K., & Lewi, E. (2021). Geothermal energy resources in Ethiopia: Status review and insights from hydrochemistry of surface and groundwaters. Wiley Interdisciplinary Reviews: Water, 8(6), e1554.
8. Teklemariam, M., Beyene, K., AmdeBerhan, Y., & Gebregziabher, Z. (2000). Geothermal development in Ethiopia. Proceedings, World Geothermal Congress 2000, 475–480.
9. Bonini, M., Corti, G., Innocenti, F., Manetti, P., Mazzarini, F., Abebe, T., & Pecskay, Z. (2005). Evolution of the Main Ethiopian Rift in the frame of Afar and Kenya rifts propagation. Tectonics, 24(1).
10. Chorowicz, J. (2005). The east African rift system. Journal of African Earth Sciences, 43(1-3), 379-410.
11. Corti, G. (2009). Continental rift evolution: from rift initiation to incipient break-up in the Main Ethiopian Rift, East Africa. Earth-Science Reviews, 96(1-2), 1-53.
12. Le Turdu, C., Tiercelin, J. J., Gibert, E., Travi, Y., Lezzar, K. E., Richert, J. P., ... & Taieb, M. (1999). The Ziway–Shala lake basin system, Main Ethiopian Rift: influence of volcanism, tectonics, and climatic forcing on basin formation and sedimentation. Palaeogeography, Palaeoclimatology, Palaeoecology, 150(3-4), 135-177.
13. Woldegabriel, G., Aronson, J. L., & Walter, R. C. (1990). Geology, geochronology, and rift basin development in the central sector of the Main Ethiopia Rift. Geological Society of America Bulletin, 102(4), 439-458.
14. Tesema, S., & Bekele, G. (2014). Resource assessment and optimization study of efficient type hybrid power system for electrification of rural district in Ethiopia. International Journal of Energy and Power Engineering, 3(6), 331-340.
15. Kebede, S. (2014). Geothermal exploration and development in Ethiopia: country update. In Short Course IX on Exploration for Geothermal Resources (Vol. 15, p. 8).
16. Kebede, S. (2016). Country update on geothermal exploration and development in Ethiopia. In Proceedings, 6th African Rift geothermal conference (pp. 1-15).
17. Kruger, W., Fezeka, S., & Olakunle, A. (2019). Ethiopia country report. Report 5: Energy and Economic Growth Research Programme (W01 and W05) PO Number: PO00022908.
18. Zemedkun, M. T. (2012). Overview of geothermal resource exploration and development in the East African rift system. Short Course VII on Exploration for Geothermal Resources, Organized by UNU-GTP, GDC and KenGen, at Lake Bogoria and Lake Naivasha, Kenya.
19. Khan, B., & Singh, P. (2017). The current and future states of Ethiopia's energy sector and potential for green energy: A comprehensive study. In International Journal of Engineering Research in Africa (Vol. 33, pp. 115-139). Trans Tech Publications Ltd.
20. Omenda, P., & Teklemariam, M. (2010). Overview of geothermal resource utilization in the east African rift system. Short Course V on Exploration for Geothermal Resources
21. Mengesha, T., Tadiwos, C., & Workneh, H. (1996). The geological map of Ethiopia, 1: 2,000,000 scale. Ethiopia: EIGS Addis Ababa.
22. Blakely, Richard J, & Simpson, R. W. (1986). Approximating edges of source bodies from magnetic or gravity anomalies. Geophysics, 51(7), 1494–1498
23. Corwin, R. F. (1990). The self-potential method for environmental and engineering applications. In Geotechnical an Environmental Geophysics: Volume I: Review and Tutorial (pp. 127-146). Society of Exploration Geophysicists.
24. Hinze, W. J. (1990). The role of gravity and magnetic methods in engineering and environmental studies. In Geotechnical an Environmental Geophysics: Volume I: Review and Tutorial (pp. 75-126). Society of Exploration Geophysicists.
25. Menke, W. (2018). Geophysical data analysis: Discrete inverse theory. Academic press.
26. Paterson, N. R., & Reeves, C. V. (1985). Applications of gravity and magnetic surveys: The state-of-the-art in 1985. Geophysics, 50(12), 2558-2594.
27. Armstead, H. C. (1982). Proposal for accelerating geothermal power development: especially for small systems. Bull., Geotherm. Resour. Counc.(Davis, Calif.);(United States), 11(8).
28. Armstead, H. C. H. (1978). Geothermal energy: its past, present and future contributions to the energy needs of man.

London.
29. Chernet, T., Hart, W. K., Aronson, J. L., & Walter, R. C. (1998). New age constraints on the timing of volcanism and tectonism in the northern Main Ethiopian Rift–southern Afar transition zone (Ethiopia). Journal of Volcanology and Geothermal Research, 80(3-4), 267-280
30. Keranen, K., & Klemperer, S. L. (2008). Discontinuous and diachronous evolution of the Main Ethiopian Rift: Implications for development of continental rifts. Earth and Planetary Science Letters, 265(1-2), 96-111.
31. Wolfenden, E., Ebinger, C., Yirgu, G., Deino, A., & Ayalew, D. (2004). Evolution of the northern Main Ethiopian rift: birth of a triple junction. Earth and Planetary Science Letters, 224(1-2), 213-228.
32. Di Paola, G. M. (1971). Geology of the Corbetti Caldera area (Main Ethiopian Rift Valley). Bulletin Volcanologique, 35(2), 497-506.
33. Mohr, P. A. (1967). The Ethiopian rift system, bulletin of the Geophys. Obs. Addis Ababa University, 11
34. Altaye, E. (1983). Preliminary Geological report of Corbetti Caldera area (with 1:50,000 Geological map), Geothermal exploration project Ministry of Mines & Energy, Addis Ababa, Ethiopia.
35. Altaye, E. (1984). Geology and surface alter-ation of Corbetti caldera area. Ethiopia, Geothermal Institute report, 84
36. Yemane, T., WoldeGabriel, G., Tesfaye, S., Berhe, S. M., Durary, S., Ebinger, C., & Kelley, S. (1999). Temporal and geochemical characteristics of Tertiary volcanic rocks and tectonic history in the southern Main Ethiopian Rift and the adjacent volcanic fields. Acta Vulcanologica, 11, 99-120.
37. Mohr, P. A. (1962). The geology of Ethiopia, 268 pp. Univ. Coll. Press, Addis Ababa.
38. WoldeGabriel, G., Heiken, G., White, T. D., Asfaw, B., Hart, W. K., & Renne, P. R. (2000). Volcanism, tectonism, sedimentation, and the paleoanthropological record in the Ethiopian Rift System. Geological Society of America Special Papers, 345, 83-99.
39. WoldeGabriel, G., Yemane, T., Suwa, G., White, T., & Asfaw, B. (1991). Age of volcanism and rifting in the Burji-Soyoma area, Amaro Horst, southern Main Ethiopian Rift: geo-and biochronologic data. Journal of African Earth Sciences (and the Middle East), 13(3-4), 437-447.
40. MoME. (1986). Geothermal exploration project Lake District, Corbetti geothermal prospect geophysical exploration, Ethiopia Project Profile, Ministry of Mines, Addis Ababa, Ethiopia.
41. Moritz, H. (1988). Geodetic reference system 1980. Bulletin géodésique, 62(3), 348-358.
42. Morelli, C., Gantar, C., McConnell, R. K., Szabo, B., & Uotila, U. (1972). The international gravity standardization net 1971 (IGSN 71). OSSERVATORIO GEOFISICO SPERIMENTALE TRIESTE (ITALY).
43. LaFehr, T. R. (1991). Standardization in gravity reduction. Geophysics, 56(8), 1170-1178
44. Montaj, G. O. (2015). Data processing and analysis systems for earth science applications (Ver. 8.3. 3). Geosoft Inc., Toronto.
45. Berrino, G., Rymer, H., Brown, G. C., & Corrado, G. (1992). Gravity-height correlations for unrest at calderas. Journal of volcanology and geothermal research, 53(1-4), 11-26.
46. Cochran, J. R., & Talwani, M. (1978). Gravity anomalies, regional elevation, and the deep structure of the North Atlantic. Journal of Geophysical Research: Solid Earth, 83(B10), 4907-4924.
47. Patre, C. D., & Williams-Jones, G. Gravity Mapping of the Mount Meager Volcanic Complex: Preliminary Results. Garibaldi Geothermal Energy Project, 50
48. Kebede, B., & Mammo, T. (2021). Processing and interpretation of full tensor gravity anomalies of Southern Main Ethiopian Rift. Heliyon, 7(4), e06872.
49. Mammo, T. (2013). Crustal structure of the flood basalt province of Ethiopia from constrained 3-D gravity inversion. Pure and Applied Geophysics, 170(12), 2185-2206.
50. Jacobsen, B. H. (1987). A case for upward continuation as a standard separation filter for potential-field maps. Geophysics, 52(8), 1138-1148.
51. Lyngsie, S. B., Thybo, H., & Rasmussen, T. M. (2006). Regional geological and tectonic structures of the North Sea area from potential field modelling. Tectonophysics, 413(3-4), 147-170.
52. Mammo, T. (2010). Delineation of sub-basalt sedimentary basins in hydrocarbon exploration in North Ethiopia. Marine and petroleum geology, 27(4), 895-908.
53. Nabighian, M. N. (1972). The analytic signal of two-dimensional magnetic bodies with polygonal cross-section: its properties and use for automated anomaly interpretation. Geophysics, 37(3), 507-517.
54. Miller, H. G., & Singh, V. (1994). Potential field tilt—a new concept for location of potential field sources. Journal of applied Geophysics, 32(2-3), 213-217.
55. Beiki, M. (2010). Analytic signals of gravity gradient tensor and their application to estimate source location. Geophysics, 75(6), I59-I74.
56. ARISOY, M. Ö., & DİKMEN, Ü. (2013). Edge detection of magnetic sources using enhanced total horizontal derivative of the tilt angle. Yerbilimleri, 34(1), 73-82.
57. Ibraheem, I. M., Gurk, M., Tougiannidis, N., & Tezkan, B. (2018). Subsurface investigation of the Neogene Mygdonian Basin, Greece using magnetic data. Pure and Applied Geophysics, 175(8), 2955-2973
58. Salem, A., Williams, S., Fairhead, J. D., Ravat, D., & Smith, R. (2007). Tilt-depth method: A simple depth estimation method using first-order magnetic derivatives. The leading edge, 26(12), 1502-1505.
59. Hutchison, W., Fusillo, R., Pyle, D. M., Mather, T. A., Blundy, J. D., Biggs, J., ... & Calvert, A. T. (2016). A pulse of mid-Pleistocene rift volcanism in Ethiopia at the dawn of modern humans. Nature Communications, 7(1), 1-12.
60. Maestrelli, D., Corti, G., Bonini, M., Montanari, D., & Sani, F. (2021). Caldera collapse and tectonics along the Main Ethiopian Rift: reviewing possible relationships. Comptes Rendus. Géoscience, 353(S2), 1-19.
61. Gottsmann, J., Biggs, J., Lloyd, R., Biranhu, Y., & Lewi, E. (2020). Ductility and compressibility accommodate high magma flux beneath a silicic continental rift caldera: Insights from Corbetti caldera (Ethiopia). Geochemistry, Geophysics, Geosystems, 21(4), e2020GC008952.
62. Lavayssière, A., Greenfield, T., Keir, D., Ayele, A., & Kend-

all, J.-M. (2019). Local seismicity near the actively deforming Corbetti volcano in the Main Ethiopian Rift. Journal of Volcanology and Geothermal Research, 381, 227–237.
63. Mickus, K., Tadesse, K., Keller, G. R., & Oluma, B. (2007). Gravity analysis of the main Ethiopian rift. Journal of African Earth Sciences, 48(2-3), 59-69.
64. Maguire, P. K. H., Keller, G. R., Klemperer, S. L., Mackenzie, G. D., Keranen, K., Harder, S., ... & Amha, M. (2006). Crustal structure of the northern Main Ethiopian Rift from the EAGLE controlled-source survey; a snapshot of incipient lithospheric break-up. Geological Society, London, Special Publications, 259(1), 269-292.
65. Colby, D. J., Pyle, D. M., Fontijn, K., Mather, T. A., Melaku, A. A., Mengesha, M. A., & Yirgu, G. (2022). Stratigraphy and eruptive history of Corbetti Caldera in the Main Ethiopian Rift. Journal of Volcanology and Geothermal Research, 107580.
66. Blakely, R. J. (1995). Potential theory in gravity and magnetic applications. Cambridge university press.
67. Hailu, A. D., & Kumsa, D. K. (2021). Ethiopia renewable energy potentials and current state. AIMS Energy, 9(1), 1-14.
68. Kebede, B., Mammo, T., & Misgie, A. (2022). Structural interpretation of Southern Main Ethiopian Rift basin using constrained full tensor gravity inversion of the basement morphology. Heliyon, e09525.
69. Kebede, H., & Alemu, A. (2022). Constrained 3D gravity interface inversion for layer structures: implications for assessment of hydrocarbon sources in the Ziway-Shala Lakes basin, Central Main Ethiopian rift. Heliyon, 8(7), e09980.
70. Kebede, H., Alemu, A., & Kevin, M. (2022). Magnetic anomaly patterns and volcano-tectonic features associated with geothermal prospect areas in the Ziway-Shala Lakes Basin, Central Main Ethiopian Rift. Geothermics, 105, 102484.
71. Kebede, H., Alemu, A., Nedaw, D., & Fisseha, S. (2021). Depth estimates of anomalous subsurface sources using 2D/3D modeling of potential field data: implications for groundwater dynamics in the Ziway-Shala Lakes Basin, Central Main Ethiopian Rift. Heliyon, 7(4), e06843.
72. Kebede, H., Alemu, A., & Fisseha, S. (2020). Upward continuation and polynomial trend analysis as a gravity data decomposition, case study at Ziway-Shala basin, central Main Ethiopian rift. Heliyon, 6(1), e03292.
73. Valenta, J., Verner, K., Martínek, K., Hroch, T., Buriánek, D., Megerssa, L. A., & Málek, J. (2021). Ground fissures within the Main Ethiopian Rift: Tectonic, lithological and piping controls. Earth Surface Processes and Landforms, 46(15), 3158-3174.